PNL-5566
UC-60
18E

Improving the Performance of Mass-Consistent Numerical Models Using Optimization Techniques

J. C. Barnard
H. L. Wegley
T. R. Hiester

September 1985

Prepared for the U.S. Department of Energy
under Contract DE-AC06-76RLO 1830

Pacific Northwest Laboratory
Operated for the U.S. Department of Energy
by Battelle Memorial Institute

Battelle

PNL-5566

PACIFIC NORTHWEST LABORATORY
operated by
BATTELLE
for the
UNITED STATES DEPARTMENT OF ENERGY
under Contract DE-AC06-76RLO 1830

Printed in the United States of America
Available from
National Technical Information Service
United States Department of Commerce
5285 Port Royal Road
Springfield, Virginia 22161

NTIS Price Codes
Microfiche A01

Printed Copy

Pages	Price Codes
001-025	A02
026-050	A03
051-075	A04
076-100	A05
101-125	A06
126-150	A07
151-175	A08
176-200	A09
201-225	A010
226-250	A011
251-275	A012
276-300	A013

PNL-5566
UC-60

IMPROVING THE PERFORMANCE OF MASS-CONSISTENT NUMERICAL MODELS USING OPTIMIZATION TECHNIQUES

J. C. Barnard
H. L. Wegley
T. R. Hiester[a]

September 1985

Prepared for the
U.S. Department of Energy
under Contract DE-AC06-76RLO 1830

Pacific Northwest Laboratory
Richland, Washington 99352

[a] FloWind Corporation
Pleasanton, California 94566

SUMMARY

This report describes a technique of using a mass-consistent model to derive wind speeds over a microscale region of complex terrain. A serious limitation in the use of these numerical models is that the calculated wind field is highly sensitive to some input parameters, such as those specifying atmospheric stability. Because accurate values for these parameters are not usually known, confidence in the calculated winds is low.

However, values for these parameters can be found by tuning the model to existing wind observations within a microscale area. This tuning is accomplished by using a single-variable, unconstrained optimization procedure that adjusts the unknown parameters so that the error between the observed winds and model calculations of these winds is minimized.

Model verification is accomplished by using eight sets of hourly averaged wind data. These data are obtained from measurements made at approximately 30 sites covering a wind farm development in the Altamont Pass area. When the model is tuned to a small subset of the 30 sites, an accurate determination of the wind speeds was made for the remaining sites in six of the eight cases. (The two that failed were low wind speed cases.) Therefore, when this technique is used, numerical modeling shows great promise as a tool for microscale siting of wind turbines in complex terrain.

CONTENTS

FIGURES

TABLES

1.0 INTRODUCTION

During the past five years, commercial wind energy development has accelerated rapidly in portions of the United States. Development has been concentrated in wind farms (clusters of wind turbines) that are often located in complex terrain. In such terrain large variations in energy production can result from fluctuations in wind that occur over relatively small distances (50 to 100 m). Wind energy development has thus generated a need for small-scale or "micrositing" tools that would identify high wind speeds over areas the size of a wind farm (about 10 km^2 or 2 mi^2). The tools must provide sufficient resolution of the wind flow over the area in three-dimensional space to discriminate clearly between suitable and unsuitable sites.

This report describes a new technique for using a mass-consistent numerical flow model as a micrositing tool. Past attempts to use such numerical models have often produced questionable, or poor, results because accurate flow simulation depends in part upon model input parameters that have been provided by educated (but often erroneous) guesswork. However, it is hypothesized here that if simultaneous short-term wind measurements are available for a small number of locations in an area of interest, a single-variable, unconstrained optimization technique can be used to calculate the important flow model parameters using available wind data. This technique should provide accurate wind-flow predictions over the entire area of interest and should not require more extensive wind data than those that would normally be collected during the wind prospecting phase of turbine siting. Studies by Kitada et al. (1983) suggest that complex flow conditions can be accurately represented using limited observed data.

Section 2 of this report provides a conceptual description of the mathematical optimization scheme and how it is used in the flow model. In Section 3 verification results for the model are presented and discussed. Recommendations for further development of an accurate micrositing tool are made in Section 4. Detailed verification data are contained in an appendix to the report.

2.0 A NEW TECHNIQUE FOR USING MASS-CONSISTENT MODELS FOR WIND FIELD CALCULATIONS

Atmospheric flow models vary greatly in complexity. Among the more simple of these are the so-called "mass-consistent" models. For a given area, these models take known observations of the wind at specific places and use these observations to calculate a wind field throughout the modeling domain. In this way, the wind can be estimated at places away from the wind observation sites. The simplicity of these models makes them attractive for wind energy purposes, as they do not require much input data, and they are easy and economical to operate.

Sherman (1978) describes the theory of the mass-consistent model. Known observations of the wind are used to construct an initial guess of the wind at every grid point in the modeled area. These initial winds are then adjusted to achieve a final wind field that satisfies the equation of mass continuity (hence the name mass-consistent model). The adjustment at grid points adjacent to solid boundaries is done so that the adjusted wind field is parallel to the boundary. Because these two features of the adjustment are important influences on wind flow in complex terrain, the mass-consistent model is particularly suited for flow simulations in such areas.

Another important feature of the adjustment is the relative weight given the adjustment in the horizontal and vertical directions. This weight is not a direct measure of atmospheric stability; rather, it is used in the model to simulate atmospheric stability and is given the symbol τ. Specifically, τ is the ratio of the vertical adjustment to the horizontal adjustment. Values of τ close to 1.0 imply a neutral atmosphere; the flow adjustment is not given preference in either the horizontal or vertical direction. Values of τ much less or greater than 1.0 imply stable or unstable atmospheres, respectively. The stability is important since the calculated winds are quite sensitive to the value of τ specified as input to the model.

Mass-consistent models have not been adequately tested to assure their suitability for wind energy purposes. Two difficulties have caused this situation: The first difficulty is that spatially dense verification data sets have not been available, particularly for microscale regions. The second difficulty is more subtle. Besides the wind observations and terrain data required for model input, one must also specify the atmospheric stability parameter τ. Model-calculated winds are quite sensitive to this parameter and even approximate values for it are usually not known. This occurs because τ cannot be physically related to common measures of the stability such as the vertical temperature gradient. Even if an empirical relationship can eventually be developed, temperature soundings are rarely available near the site in question. Kitada et al. (1983) discuss the sensitivity of calculated flow fields to the stability.

Since model-calculated winds are sensitive to the stability and appropriate values for it can only be guessed, confidence in calculated winds has been low. The technique to be described circumnavigates the need for a priori knowledge of the stability. Instead of being an input parameter, it becomes a calculated quantity.

The technique merges an existing mass-consistent model with an optimization procedure. (This combination will henceforth be referred to as the "model"). The model requires as input a number of wind observations over the microscale area of interest. These observations are known as "tuning" sites. One of these tuning sites is designated as the reference site and is used to initialize the model. The optimization procedure is then used to vary τ (and the wind direction of the reference site) until the error between the calculated and observed winds at the tuning sites is minimized. If this error is small, then model-derived estimates of the wind away from the wind observations should be good. The results shown later in Section 3 confirm that, when the error between calculated and observed winds at the tuning sites is small, the accuracy of model-estimated winds is high.

A mathematical description of this optimization is as follows. Assume that there are N wind observation sites distributed over a microscale region. (For the verification studies described later, N ranges from 6 to 8.) The station with the highest average wind speed is designated as the reference site. For a given averaging period (hourly averaged data are used in this report), the wind speeds are normalized by the reference site wind speed. This gives a set of ratios r_i^o for each set of (hourly) averaged wind data, where the subscript i denotes the station i and o denotes that these are observed ratios. The reference site (i=1) speed is normalized by itself so that $r_i^o = 1$.

A corresponding set of calculated ratios can be derived by operating the model with a given set of input data and then normalizing the calculated speeds of the tuning sites by the calculated speed at the reference site. These ratios are denoted by r_i^c (where c denotes calculated ratio); they are considered a function of only the atmospheric stability τ, and the input wind direction θ. The input wind direction is included since it was only crudely specified in the wind data used in this study, and variations about the given direction were sometimes observed to cause large changes in r_i^c.

It is not necessary to restrict the dependence of r_i^c to just stability and wind direction. Other parameters could also be included. The important point is to include those parameters for which the ratios r_i^c show greatest sensitivity. Initial testing has indicated that the calculated ratios are most sensitive to τ and θ. To show the explicit dependence of r_i^c on these quantities, they will be written as $r_i^c(\tau,\theta)$.

A measure of the goodness of fit between the calculated and observed ratios is the root mean square error, RSME, given by the expression

$$\mathrm{RSME}(\tau,\theta) = \left[\sum_{c=2}^{N} \; r_i^o - r_i^c(\tau,\theta)^{\;2} / (N - 1)\right]^{1/2}$$

Since the calculated ratios $r_i^c(\tau,\theta)$ depend upon τ and θ, the error is also a function of these quantities as is explicitly indicated above (the sum in the above expression does not include the reference site i=1 since it does not contribute to the error).

The root mean square error can be depicted as a three-dimensional surface. For one of the data sets used in this study, this surface is shown in Figure 2.1. The abscissae for this figure are the wind direction and the log

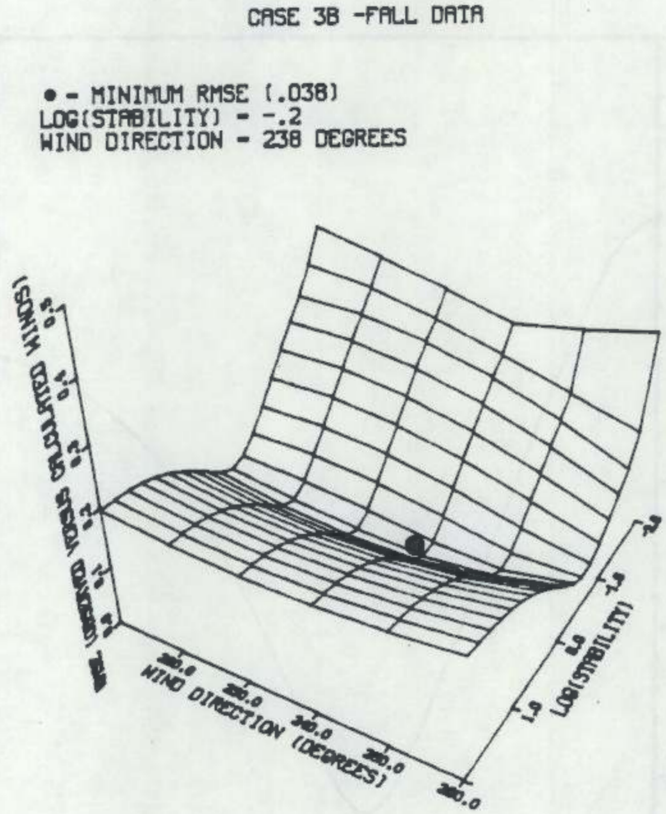

FIGURE 2.1. Sensitivity of RMSE to Stability and Wind Direction

of the stability (log (τ)), which ranges from -2 (stable) through 0 (neutral) to +2 (unstable). Figure 2.1 shows that for this particular data set the root mean square error is much more sensitive to changes in τ than to changes in the wind direction. (To better illustrate the sensitivity of RMSE(τ,θ) to stability, Figure 2.2 shows RSME(τ,θ) as a function of log(τ) for a fixed value of θ, (238°)).

The "best fit" of the observed and calculated ratios is obtained when RSME(τ,θ) is a minimum. The error is minimized in practice by making initial guesses of τ and θ and then using a single variable, unconstrained optimization technique (applied twice) to find the optimum values of these parameters; that is, the values of τ and θ when RMSE(τ,θ) is a minimum. This method is very

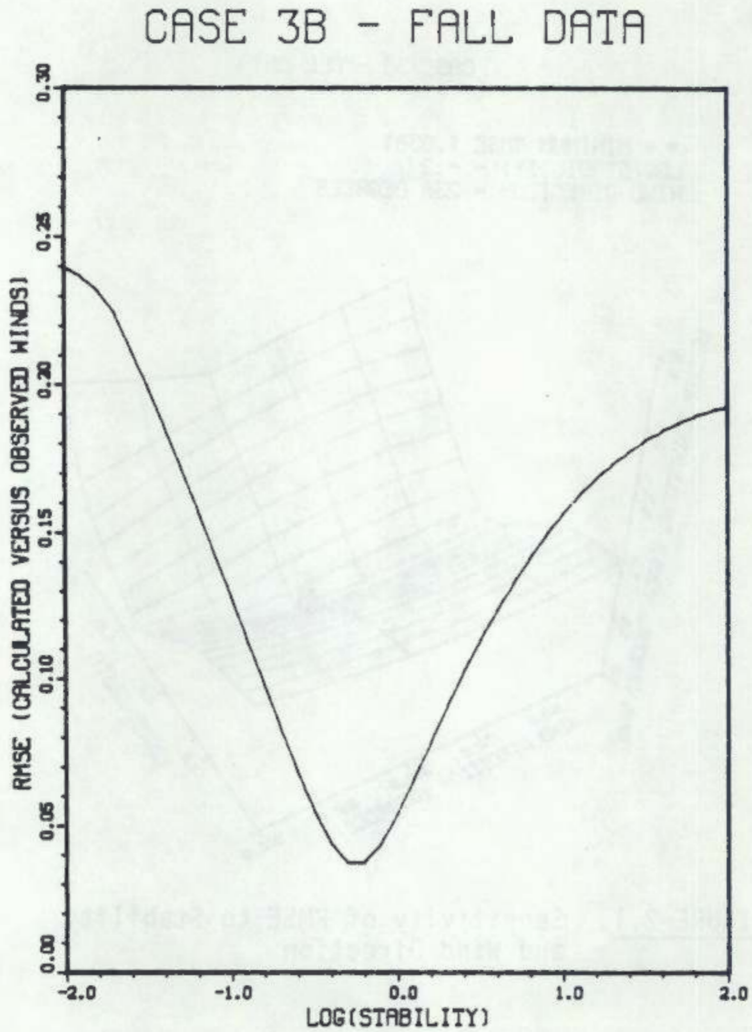

FIGURE 2.2. Sensitivity of RMSE to Stability

similar to the Coggin algorithm (Kuester and Mize 1973). For the data depicted in Figure 2.1, the minimum error occurs for $\log(\tau) = -0.2$ and $\theta = 238°$. This minimum point is indicated by the black dot on the surface. About 1 hour of VAX 11/780 computer time is required for the minimization procedure.

In summary, this technique minimizes the error between wind observations and model calculations of the wind at the tuning sites. This minimization is a function of two variables: τ and θ. If the minimum error is sufficiently small, the results in the next section show that estimates of the wind ratios away from the observation sites are good, and a priori knowledge of the stability parameter is no longer necessary.

The mass-consistent model that was merged with the optimization scheme is the NOABL model. This mass-consistent model was developed for the U.S. Department of Energy by Science Applications, Inc. A description of the model is contained in a report by Traci et al. (1978).

3.0 MODEL VERIFICATION

In this section the data set used in the verification is described, the experimental technique used is presented, and results are discussed.

3.1 DATA USED IN VERIFICATION

Data available for the verification of the flow model consisted of hourly averaged wind speed and direction at 1 reference site and simultaneous hourly averaged wind speeds for up to 27 other sites. These data were collected for the 8 cases shown in Table 3.1. Wind directions are all from the southwest quadrant (225 to 250°), the prevailing power-producing wind direction for the area. The speeds vary from light to moderate (10 to 19 mph in Case 2B) to very strong (22 to 44 mph in Case 3A).

Atmospheric stability (inferred from wind speed and time of day) appears to vary somewhat over the 8 cases. Cases 4B and 5B represent moderate and strong nighttime winds, respectively; Cases 2A and 3A represent moderate and strong afternoon winds, respectively; and Cases 4A and 5A represent moderate and strong evening winds, respectively. Thus, the data set tests to some degree the selection of appropriate stability parameters by the optimization scheme.

Figure 3.1 presents the terrain configuration and the location of the data sites for the verification of the flow model. The terrain, represented by the 20-ft contours in the figure, is based upon a 40-by-40 grid of terrain heights spaced evenly at 50-m intervals. The flow model run time increases exponentially with grid size. The 50-m grid interval was a subjectively selected value based upon an attempt to minimize the number of grid points and yet retain enough terrain resolution to represent the features that might affect the wind flow over the area. (The selection of optimal grid spacing can be made much more objective after sensitivity testing of verified model results to grid interval is accomplished.)

TABLE 3.1. Wind Data Used for Model Verification

Case Descriptions

Case	Date-Time		Wind at Reference Site Speed (mph)	Wind at Reference Site Direction (°)
2A	Oct 30	1500-1600	22	250
2B	Nov 13	1100-1200	19	240
3A	Oct 26	1400-1500	44	225
3B	Nov 2	1500-1600	41	240
4A	Oct 27	1900-2000	19	240
4B	Nov 1	2300-2400	22	250
5A	Oct 26	1900-2000	38	230
5B	Nov 13	0200-0300	41	235

Site Ref. Number	Wind Speeds (mph) by Case 2A	2B	3A	3B	4A	4B	5A	5B
1 (a)	22	19	44	41	19	22	38	41
2	18	12	29	25	18	15	28	20
3	16	10	24	23	14	20	25	21
4	17	11	27	24	15	20	27	21
5	17	12	22	31	19	17	31	23
6 (a)	19	13	30	27	17	21	28	24
7 (a)	19	13	31	28	21	20	30	24
8	21	14	35	31	22	20	33	27
9	20	--	32	29	19	20	31	--
10	17	10	24	22	14	18	23	18
11	17	11	25	23	14	20	25	21
12	17	10	26	22	15	17	25	16
13	15	11	25	23	12	19	25	21
14 (a)	17	--	29	26	12	17	25	--
15 (a)	18	12	27	26	16	19	26	20
16	16	12	25	24	15	17	26	23
17	17	12	27	24	15	17	27	21
18	17	14	29	28	16	17	28	27
19	16	14	30	28	11	17	26	27
20 (a)	18	14	--	30	--	17	--	28
21	18	13	--	31	--	16	--	27
22 (a)	17	--	34	30	11	16	28	--
23	20	16	--	33	--	20	32	32
24	18	16	35	30	16	18	30	28
25	15	13	34	32	16	16	30	28
26	19	17	40	35	15	18	32	38
27 (a)	21	19	44	39	19	20	36	36
28	21	17	42	35	18	18	33	34

(a) Tuning sites - Site 1 is the reference site.

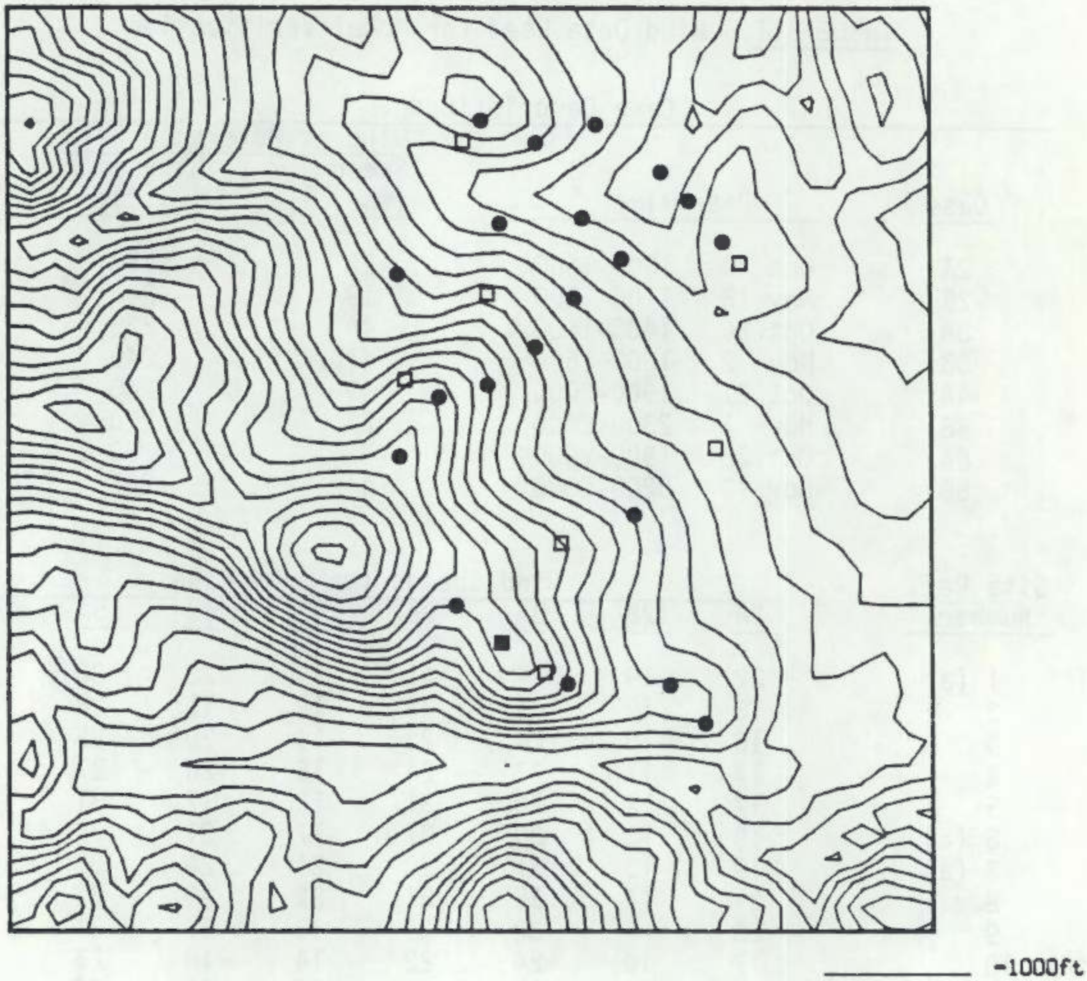

FIGURE 3.1. 20-Ft Terrain Contours and Data Site Locations

3.2 EXPERIMENTAL TECHNIQUE

To test the hypothesis that limited observations can be used to optimize the choice of flow model parameters, the 28 sites in Figure 3.1 were divided into a set of 8 tuning sites (shown as squares) and 20 verification sites (shown as filled circles). Table 3.1 summarizes the data used for model testing and verification.

One tuning site was selected as the reference site. This site is shown as a filled square in Figure 3.1. Model parameters were optimally adjusted for each of the 8 cases using all or most of the 8 tuning sites and by employing the optimization procedure described in Section 2. In 2 of the 8 cases, only 6 of the tuning sites were available and in 3 of the 8 cases, only 7 tuning sites were available. Based upon the results described later in this section, the variation in the number of sites available for optimizing (from 6 to 8) had no noticeable effect upon the model performance. A lower bound on the number of sites required to adequately tune the model for a given terrain area has not yet been established.

To create a set of calculated data for model verification, the optimally adjusted three-dimensional flow field for each case was saved. Each flow field was used to interpolate in three dimensions to obtain wind speeds for the verification sites. Since many wind farm developers have come to use wind-speed ratios (to a reference site), speed ratios were calculated using Site 1 in Table 3.1 as the reference site.

3.3 RESULTS

The results of the model tuning procedure for the 8 wind cases examined are presented in Table 3.2. Correlation coefficients (r^2) and root mean square errors (RMSEs) were used as measures of the goodness of fit of the modeled to observed wind-speed ratios. The correlation coefficient represents the fraction of the variance in the observed wind-speed ratios that is explained by the model-produced wind-speed ratios.

TABLE 3.2. RMS Error and Correlation Coefficients for Tuning Sites

	Case Description			
Case	Time	Dir(°)/ Speed (mph)	R-Squared (%)	RMSE of Ratios
2A	Day	250/22	72.4	0.042
2B	Day	240/19	92.3	0.042
3A	Day	225/44	90.9	0.045
3B	Day	240/41	93.8	0.034
4A	Eve	240/19	5.45	0.126
4B	Night	250/22	39.8	0.075
5A	Eve	230/38	84.7	0.048
5B	Night	235/41	91.0	0.056
All 8 Cases			80.0	0.065
6 Cases (excluding 4A and 4B)			90.7	0.044

Two of the 8 cases shown in the table, Cases 4A and 4B, exhibit a relatively poorer fit to the observed data. Implications of this lack of fit, or poor tuning of the model, are discussed later in this section.

Wind direction data were only available for the reference site; consequently, quantitative verification of the model-calculated directions is not presented. However, the model-derived directions appear realistic over the entire grid, and they agree well with the observed direction at the reference site.

Table 3.3 contains the complete verification data for all 8 cases examined. Comparison of these data with the tuning site data in Table 3.2 reveals that there is a slight deterioration in accuracy for the 6 well-tuned cases; however, there is a much larger deterioration for the 2 poorly tuned cases (4A and 4B). A comparison of the 6 cases, excluding 4A and 4B, shows that the overall RMSE for the verification sites is reduced to 0.037. This value is smaller than that for any individual case, which is expected since random errors between model-calculated winds and wind observations tend to cancel when averages are

TABLE 3.3. RMS Error and Correlation Coefficients for Verification Sites

Case	Case Description: Time	Case Description: Dir(°)/ Speed (mph)	R-Squared (%)	RMSE of Ratios
2A	Day	250/22	13.1[a]	0.080
2B	Day	240/19	91.3	0.060
3A	Day	225/44	84.8	0.074
3B	Day	240/41	81.0	0.050
4A	Eve	240/19	12.3	D.175
4B	Night	250/22	22.7	0.154
5A	Eve	230/38	62.3	0.047
5B	Night	235/41	78.0	0.067
All 8 Cases			48.2	0.099
6 Cases (excluding 4A and 4B)			81.2	0.037

(a) The low R-squared is caused by a single outlying point.

taken. Figure 3.2, a scatter plot of observed versus modeled ratios for the 6 well-tuned cases, clearly demonstrates the skill of the flow model when proper values of the input parameters are selected.

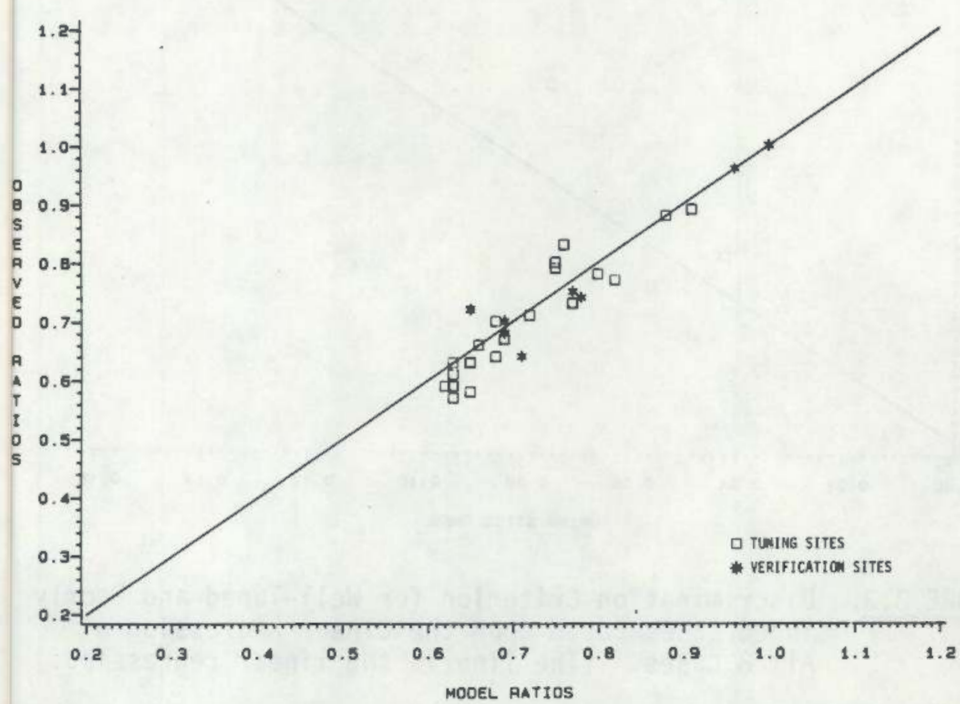

FIGURE 3.2. Tuning and Verification Site Observed Versus Modeled Wind-Speed Ratios for the Six Well-Tuned Cases

Explanations for the poorer performance of the tuning procedure for Cases 4A and 4B are still being explored; however, it is important to note that cases of poor tuning results can be identified during the tuning procedure to warn the user that the results of a particular model run may not be accurate. For example, in Figure 3.3 the correlation between tuning site RMSEs and verification site RMSEs demonstrates that, for the 8 cases examined, the tuning site RMSE of about 0.06 can be used to discriminate between good and poor model results. For the majority of cases examined, the flow model results were good to excellent.

To further illustrate the differences between expected (good) model performance and poor performance, scatter plots of wind-speed ratios are presented

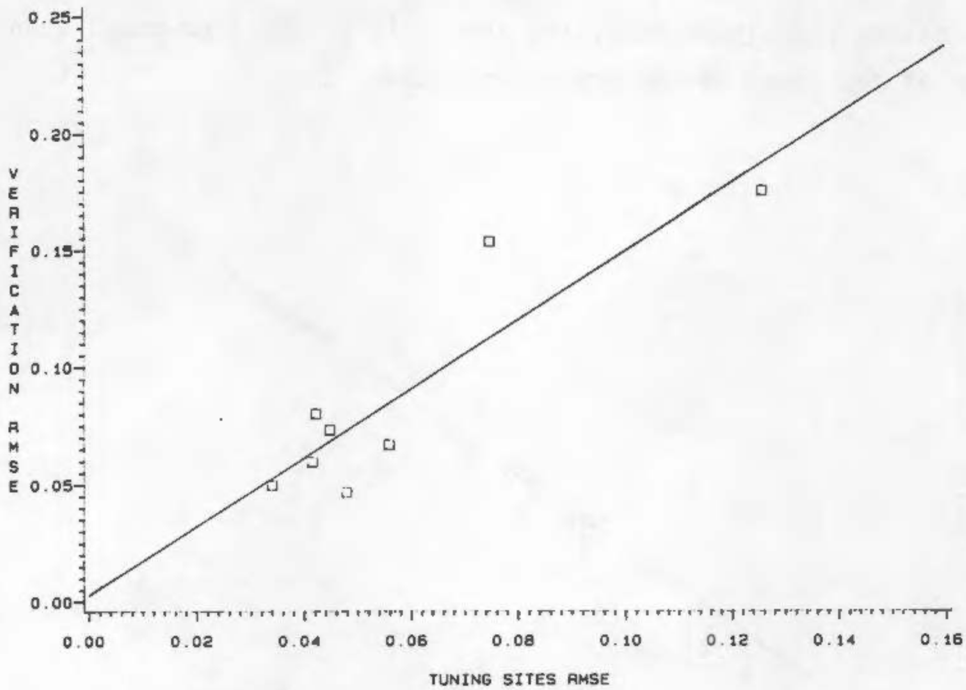

FIGURE 3.3. Discrimination Criterion for Well-Tuned and Poorly Tuned Cases Based Upon the Linear Regression of All 8 Cases. (The line is the linear regression.)

in Figures 3.4 and 3.5, respectively, for a typically well-tuned case (Case 3A) and a poorly tuned case (Case 4A).

It is noteworthy that the flow model was poorly tuned only in cases where the winds were light to moderate (i.e., 10 to 20 mph) over the area of interest. Even when the model was well tuned and performed well (as in Figure 3.4), at the lower wind speeds the model tended to overpredict the ratios. For example, in Figure 3.4 calculated ratios between 0.5 and 0.7 were about 10% too high. The overprediction may not be due solely to the assumption of mass consistency. This effect could be partially due to the nature of the objective function (the root mean square error) that is minimized during the tuning process. The squaring of errors tends to weight the larger errors occurring at higher wind speeds more heavily than relatively smaller errors at the lower wind speeds. Consequently, the model tuning is biased toward the higher wind speeds.

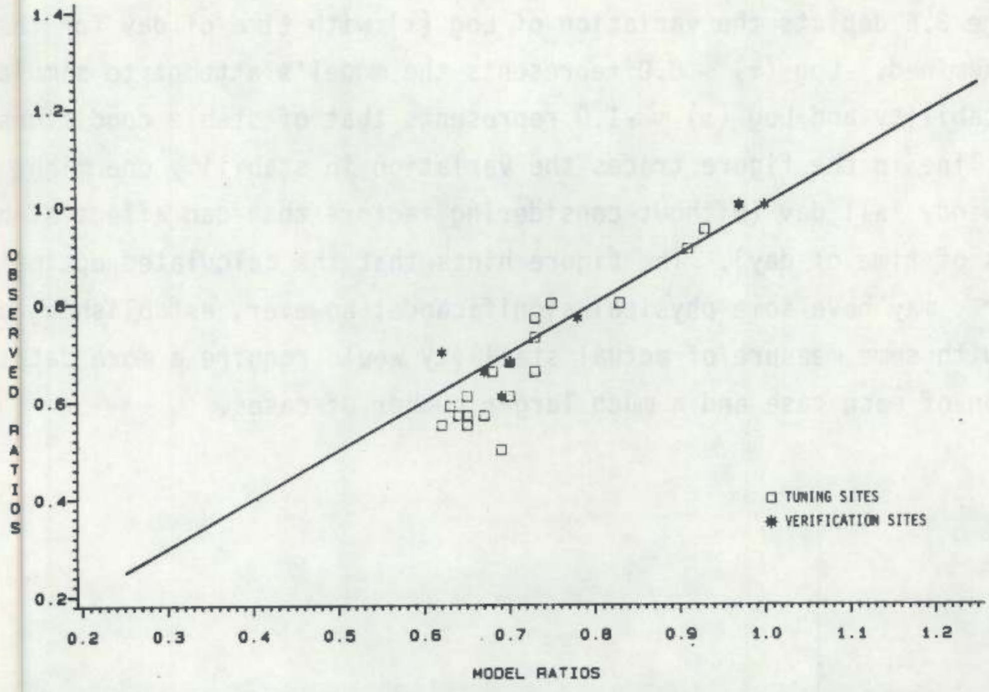

FIGURE 3.4. Typical Well-Tuned Flow Model Results (Case 3A)

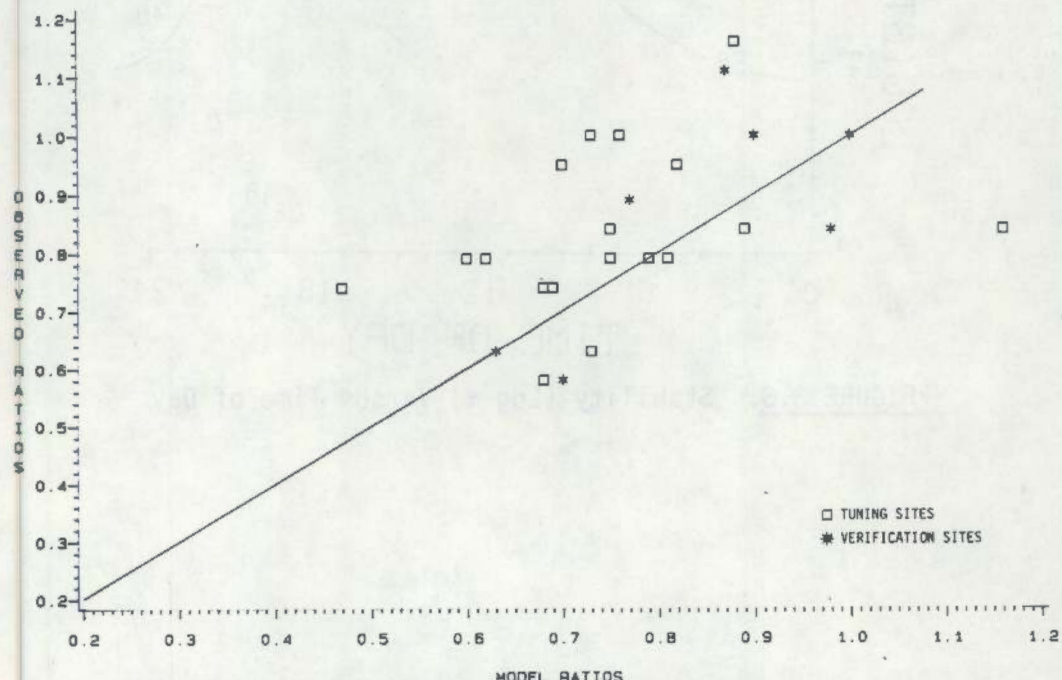

FIGURE 3.5. A Typical Case Demonstrating Poorly Tuned Flow Model Results (Case 4A)

Figure 3.6 depicts the variation of Log (τ) with time of day for the 8 cases examined. Log (τ) $\sim$ 0.0 represents the model's attempt to simulate neutral stability and Log (τ) $\sim$ -1.0 represents that of stable conditions. The solid line in the figure traces the variation in stability one might expect during a windy fall day (without considering factors that can affect stability regardless of time of day). The figure hints that the calculated optimal values for τ may have some physical significance; however, establishing a relationship with some measure of actual stability would require a more detailed examination of each case and a much larger number of cases.

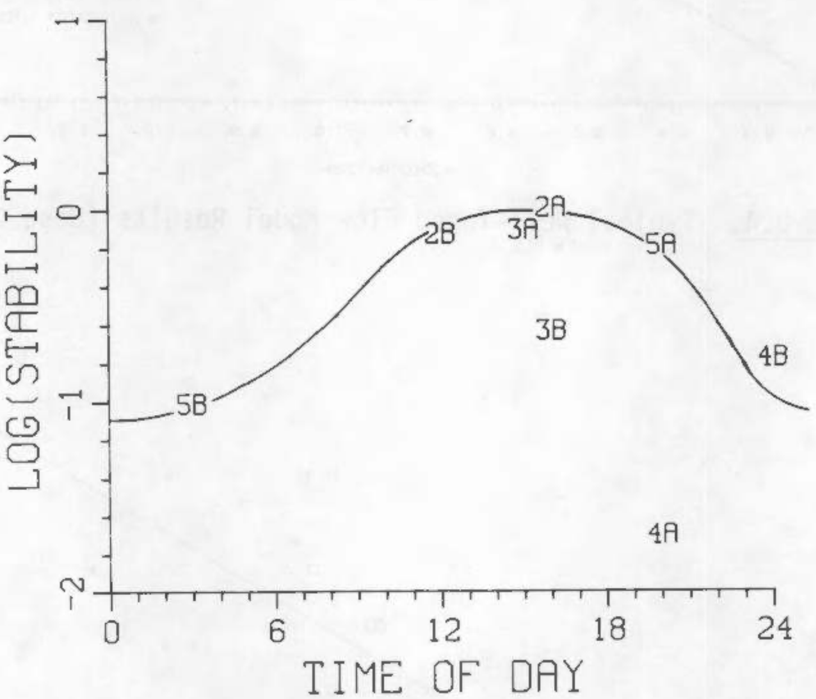

FIGURE 3.6. Stability (Log τ) Versus Time of Day

4.0 FURTHER RESEARCH

The results presented in Section 3 are promising and suggest that numerical modeling can play a useful role in micrositing. Because the model was verified using only 8 data sets, there is not yet enough evidence to establish the model's reliability. Much more testing is necessary.

Further testing should be targeted at resolving the major uncertainty: Will the model perform well over a wide range of wind speeds and when applied to many different regions of complex terrain? Testing designed to investigate this would require large data sets obtained from spatially dense wind measurement programs undertaken at different places. Model performance can be gauged by the comparison of model results to the observations.

It is of particular importance to determine the range of wind speeds over which the model performs well. The results of Section 3 indicate that poor results sometimes occur for low wind speeds. This is physically plausible since physical factors aside from nondivergence assume a more dominant role at lower speeds. Unfortunately, the results achieved to date are too limited to permit a lower bound on the wind speed range to be established. The value of this bound is critical since if it is significantly greater than typical turbine cut-in speeds, some of the usefulness of the model will be lost.

Also of importance is the number of wind observations required for model initialization. Acceptable results were achieved for most cases presented in this report by using from 6 to 8 stations. It is not known if results of similar accuracy will still occur if the number of initialization stations is reduced. Also, the poor results (of Cases 4A and 4B) may be improved by using more stations. An additional goal of testing is then to establish guidelines on the initialization requirements depending upon the wind speed and other conditions. The use of wind direction at all tuning sites in addition to wind speed may enhance the results or reduce the number of initialization stations; this should also be investigated.

5.0 REFERENCES

Kitada, T., A. Kaki, H. Ueda, and L. K. Peters. 1983. "Estimation of Vertical Air Motion from Limited Horizontal Wind Data - A Numerical Experiment." Atmospheric Environment, 17:2181-2192.

Kuester, J. L., and J. H. Mize. 1973. Optimization Techniques with Fortran. McGraw-Hill, New York, New York.

Sherman, C. A. 1978. "A Mass-Consistent Model for Wind Fields over Complex Terrain." J. Appl. Meteor., 17:312-319.

Traci, R. M., G. T. Phillips, and P. C. Patnaik. 1978. Developing a Site Selection Methodology for Wind Energy Conversion Systems. DOE/ET/20280-3, National Technical Information Service, Springfield, Virginia.

APPENDIX

MODEL VERIFICATION RESULTS FOR EIGHT WIND CASES EXAMINED

APPENDIX

MODEL VERIFICATION RESULTS FOR EIGHT WIND CASES EXAMINED

The following eight figures are scatter plots of model-calculated versus observed wind speed ratios for both the tuning and verification sites listed in Table 3.1 in the main body of the report. All ratios are calculated using Site 1 (in Table 3.1) as the reference site (denominator). The eight cases are those described in Table 3.1.

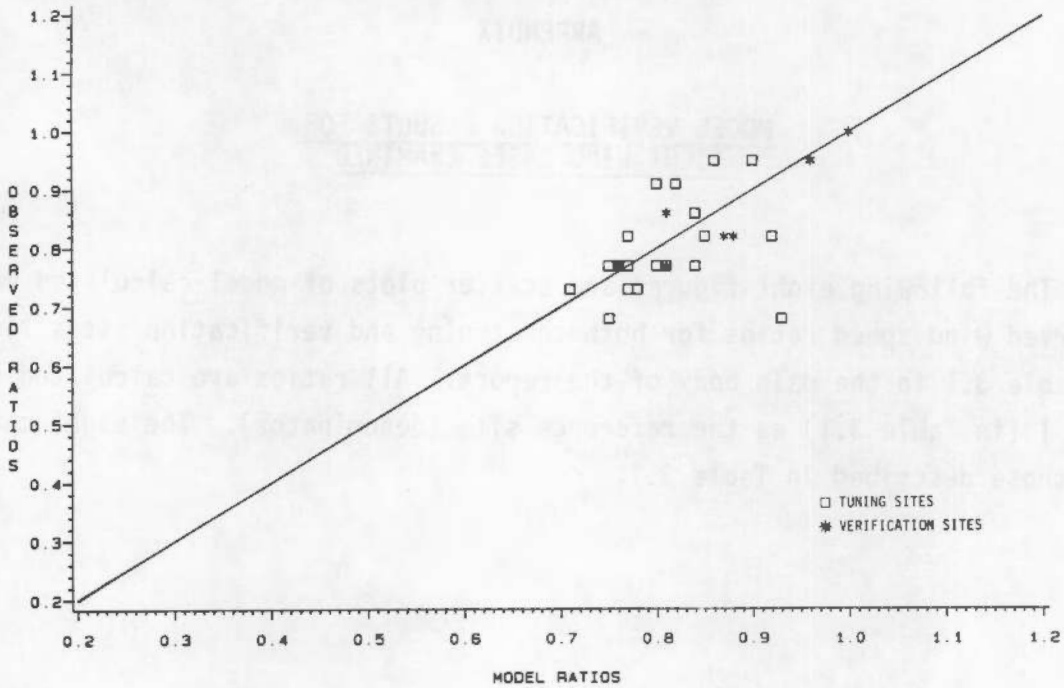

FIGURE A.1. Scatter Plot of Observed Versus Model-Calculated Wind Speed Ratios for Case 2A

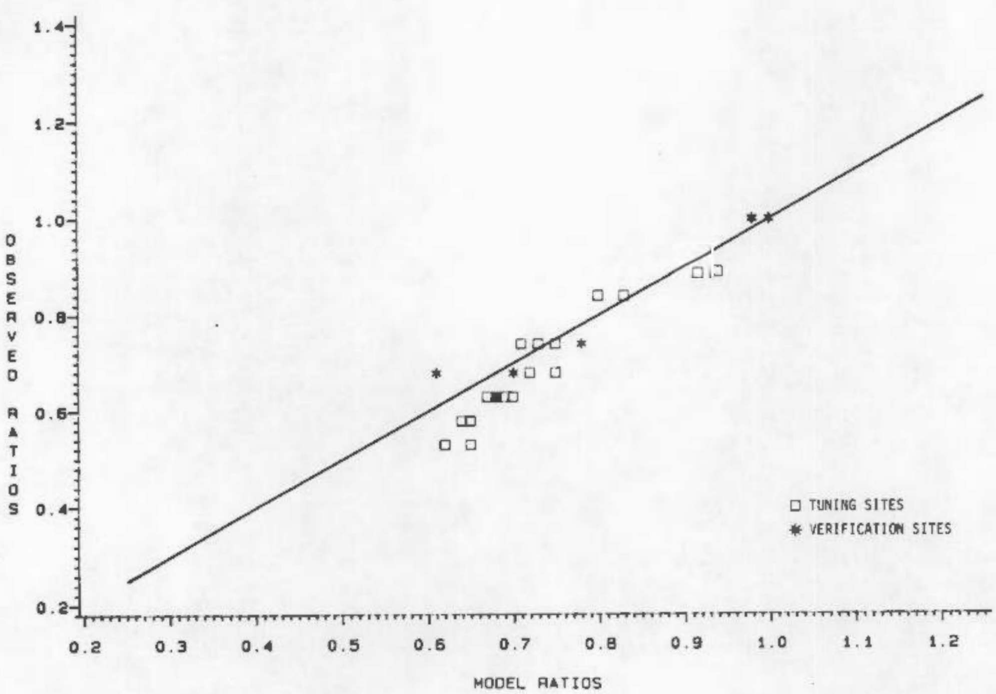

FIGURE A.2. Scatter Plot of Observed Versus Model-Calculated Wind Speed Ratios for Case 2B

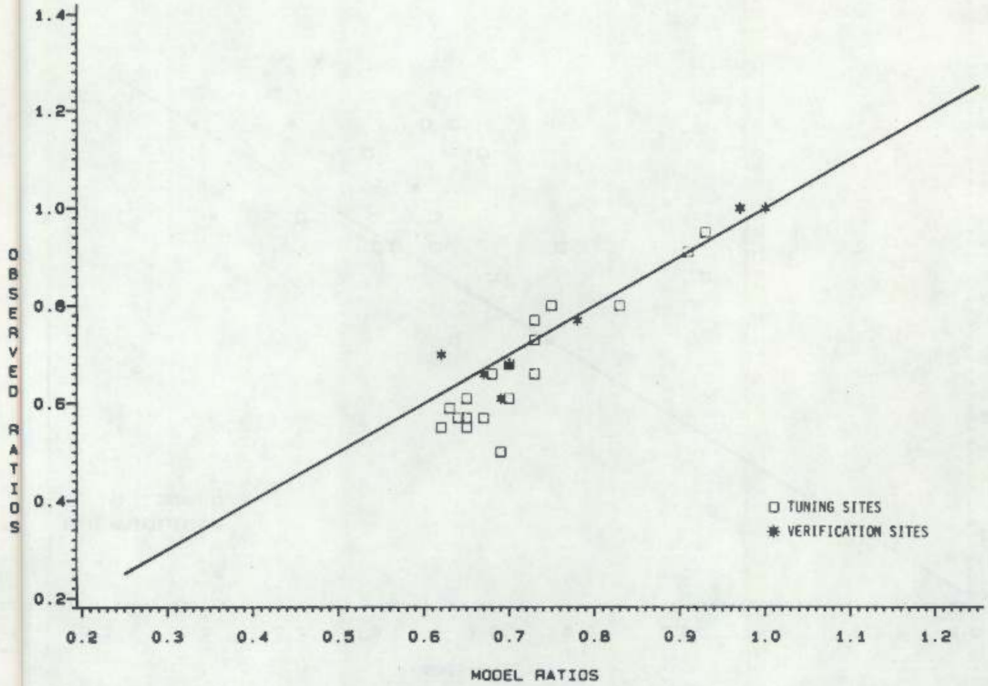

FIGURE A.3. Scatter Plot of Observed Versus Model-Calculated Wind Speed Ratios for Case 3A

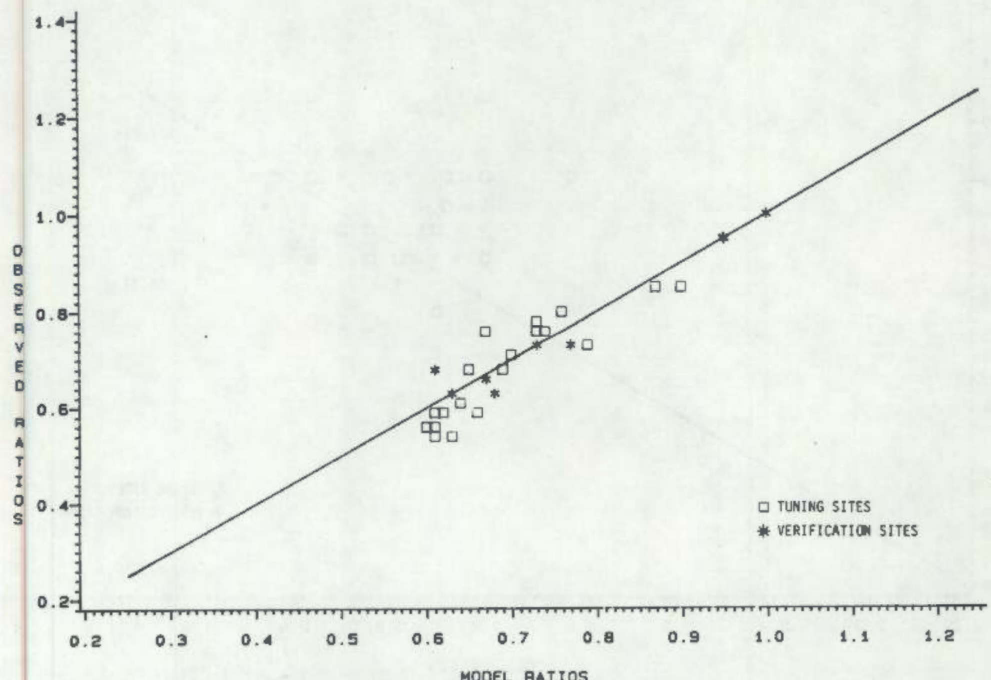

FIGURE A.4. Scatter Plot of Observed Versus Model-Calculated Wind Speed Ratios for Case 3B

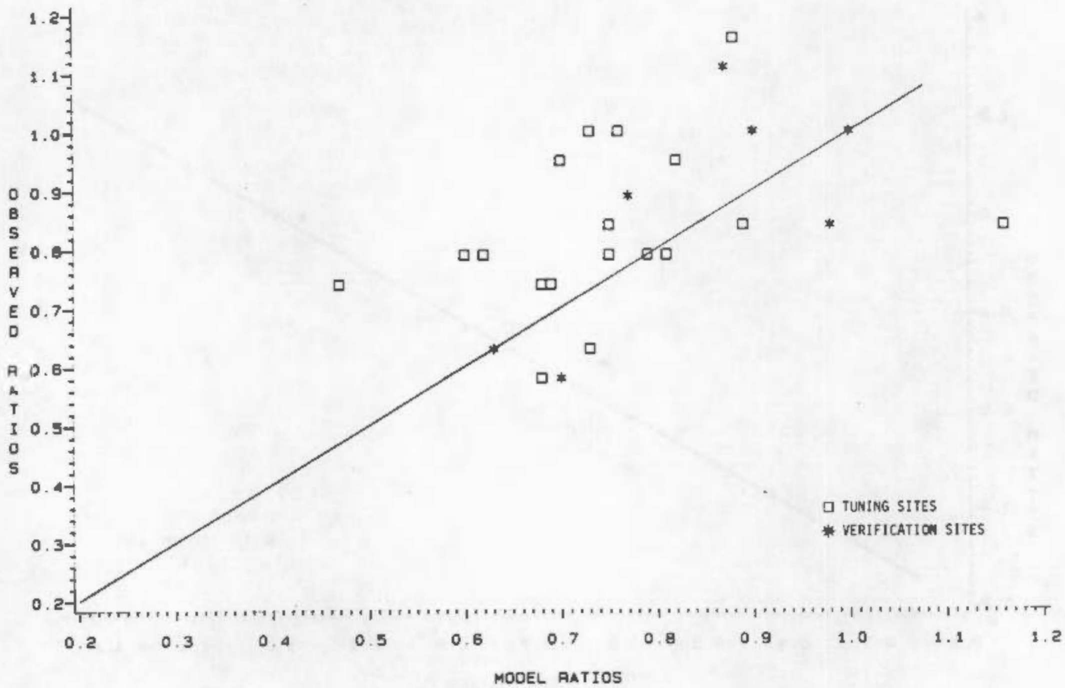

FIGURE A.5. Scatter Plot of Observed Versus Model-Calculated Wind Speed Ratios for Case 4A

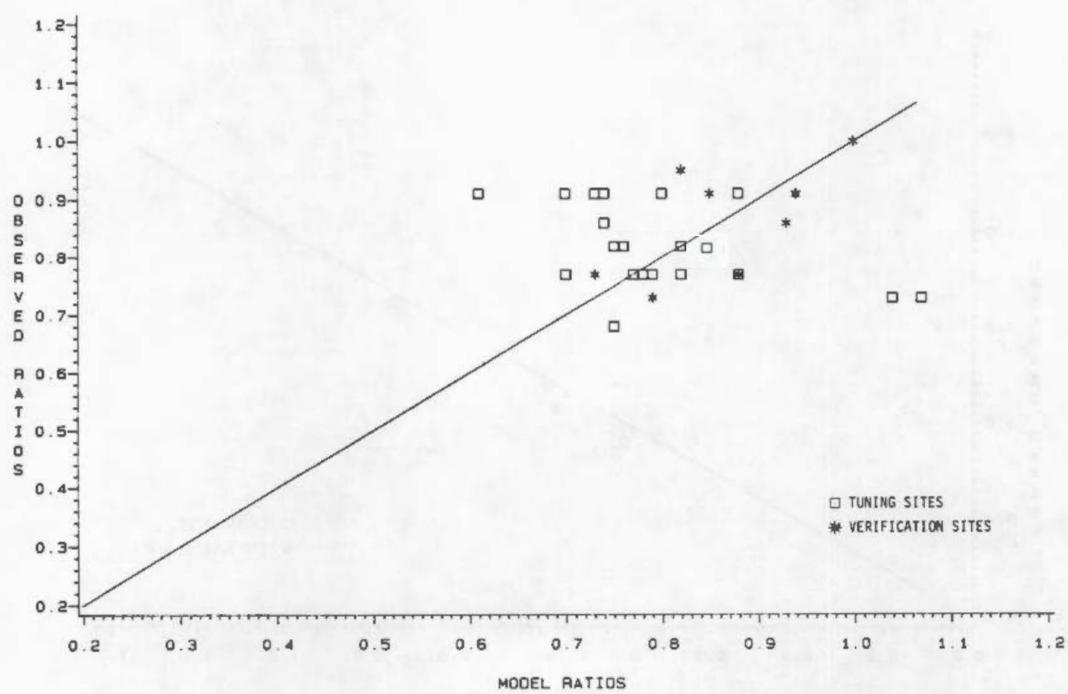

FIGURE A.6. Scatter Plot of Observed Versus Model-Calculated Wind Speed Ratios for Case 4B

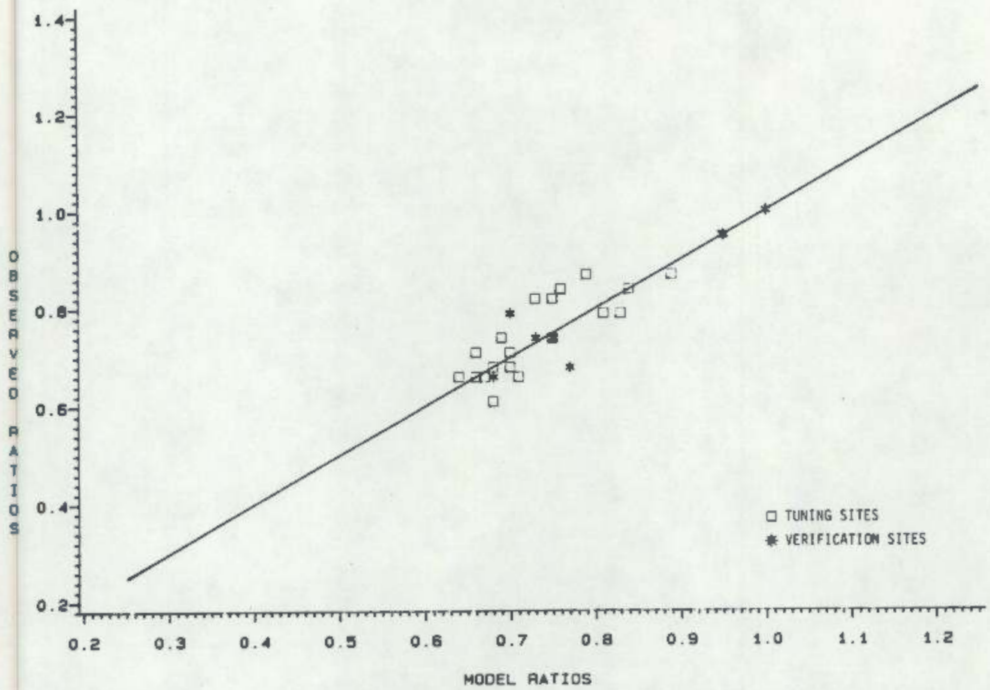

FIGURE A.7. Scatter Plot of Observed Versus Model-Calculated Wind Speed Ratios for Case 5A

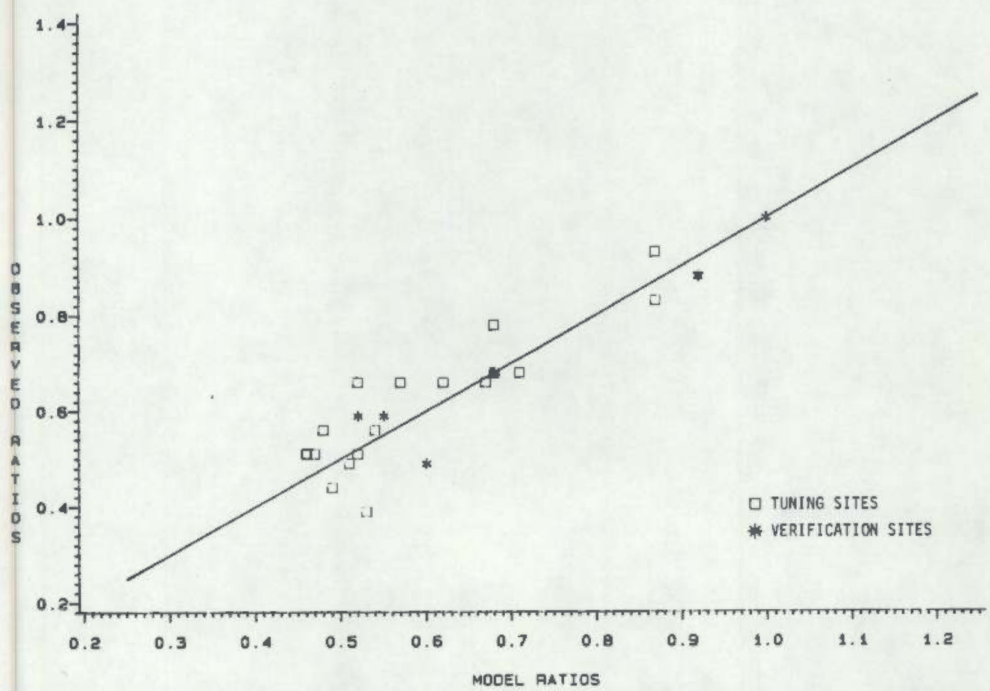

FIGURE A.8. Scatter Plot of Observed Versus Model-Calculated Wind Speed Ratios for Case 5B

DISTRIBUTION

No. of Copies	

OFFSITE

Carl Aspliden
Battelle Memorial Institute
Washington Office
2030 M Street NW
Washington, DC 20036

J. Cadogan
Department of Energy
Wind Energy Technology Division
1000 Independence Avenue
Forrestal Building, Room 5H048
Washington, DC 20585

O. F. Ancona
Department of Energy
Wind Energy Technology Division
1000 Independence Avenue
Forrestal Building, Room 5H048
Washington, DC 20585

G. P. Tennyson
Department of Energy
Albuquerque Operations Office
P.O. Box 5400
Albuquerque, NM 87110

30 DOE Technical Information Center

Peter Lissaman
Aerovironment, Inc.
145 Vista Avenue
Pasadena, CA 91107

Tom Gray
American Wind Energy Association
1516 King Street
Alexandria, VA 22314

W. A. Vachon
P.O. Box 149
Manchester, MA 01944

Mike Bovarnick
Boeing Aerospace Corporation
P.O. Box 3999
Seattle, WA 98124

Wayne Wiesner
Boeing Aerospace Corporation
P.O. Box 3999
Seattle, WA 98124

Gary Miller
Boeing Aerospace Corporation
P.O. Box 3999
Seattle, WA 98124

Mike Rees
Boeing Aerospace Corporation
PO Box 3999
Seattle, WA 98124

Don Fries
Boeing Aerospace Corporation
P.O. Box 3999
Seattle, WA 98124

Dick Hacker
Boeing Aerospace Corporation
P.O. Box 3999
Seattle, WA 98124

Ron Holeman
Bonneville Power Administration
Generation Engineering
P.O. Box 3621
Portland, OR 97208

S. J. Hightower
Bureau of Reclamation
Denver Federal Center
Building 67, Code 254
Denver, CO 80225

Willi Sadeh
Department of Civil Engineering
Colorado State University
Fort Collins, CO 80523

No. of
Copies

V. A. Sandborn
Department of Civil
Engineering
Colorado State University
Fort Collins, CO 80523

Dr. Edgar DeMeo
Electric Power Research
Institute
3412 Hillview Avenue
Palo Alto, CA 94303

Frank Goodman, Jr.
Electric Power Research
Institute
3412 Hillview Avenue
Palo Alto, CA 94303

R. L. George
TERRA Sciences, Inc.
7555 W. 10th Avenue
Lakewood, CO 80214

Tom Hiester
FloWind Corporation
1183 Quarry Lane
Pleasanton, CA 94566

J. M. Kos
Hamilton Standard
Bradley Field Road
Windsor Locks, CT 06096

Eugene Di Valentin
Hamilton Standard
Bradley Field Road
Windsor Locks, CT 06096

Glid Doman
Hamilton Standard
Bradley Field Road
Windsor Locks, CT 06096

G. L. Park
Department of Electrical
Engineering
Michigan State University
East Lansing, MI 48824

No. of
Copies

R. B. Schlueter
Department of Electrical
Engineering
Michigan State University
East Lansing, MI 48824

W. D. Johnston
Hawaiian Electric Company, Inc.
P.O. Box 2750
Honolulu, HI 96840

David Spera
NASA/Lewis Research Center
21000 Brookpark Road
Cleveland, OH 44135

Phillip French
NASA Scientific and Technical
Information Facility
P.O. Box 8757
Baltimore/Washington International
Airport
Baltimore, MD 21240

J. C. Kaimal
National Oceanic and Atmospheric
Administration/Environmental
Research Laboratories/Wave
Propagation Laboratory
3000 Marine Street
Boulder, CO 80302

G. M. Gregorek
Aeronautics and Astronautics
Research Lab
Ohio State University
2300 W. Case Road
Columbus, OH 43220

Peter M. Moretti
Oklahoma State University
Mechanical and Aerospace
Engineering
Engineering North 218
Stillwater, OK 74074

No. of
Copies

Robert Wilson
Department of Mechanical Engineering
Oregon State University
Corvallis, OR 97331

Dr. H. A. Panofsky
6222 Agee Street #5
San Diego, CA 92122

J. Dutton
Department of Meteorology
Pennsylvania State University
University Park, PA 16902

Andrew Trenka
Solar Energy Research Institute
Rocky Flats
P.O. Box 464
Golden, CO 80401

P. Klimas
Sandia Laboratories
Division 5443, P.O. Box 5800
Albuquerque, NM 87115

Robert Noun
Solar Energy Research Institute
1617 Cole Boulevard
Golden, CO 80401

Robert Thresher
Solar Energy Research Institute
1617 Cole Boulevard
Golden, CO 80401

Sherman M. Chan
Systems Control, Inc.
1801 Page Mill Road
P.O. Box 10025
Palo Alto, CA 94303

R. H. Kirchhoff
Department of Mechanical Engineering
University of Massachusetts
Amherst, MA 01003

No. of
Copies

Earl L. Davis
U.S. Windpower, Inc.
2305 S. Vasco Road
Livermore, CA 94550

H. Tieleman
Department of Engineering Science & Mechanics
Virginia Polytechnic Institute and State University
Blacksburg, VA 24061

Susan Hosch
Washington State Energy Office
400 E. Union Avenue, 1st Floor
Olympia, WA 98504

Farrell Smith Seiler
Wind Energy Report
Box 14 - 104 S. Village Avenue
Rockville Centre, NY 11571

FOREIGN

Leif Kristensen
Department of Physics
Risø National Laboratory
4000 Roskilde
DENMARK

Per Lundsager
Risø National Laboratory
P.O. Box 49
DK-4000 Roskilde
DENMARK

Dr. M. B. Anderson
Sir Robert McAlpine & Sons, Ltd.
40 Bernard Street
London WC1N 1LG
ENGLAND

Dr. D. Wilson
Cavendish Laboratory
Madingley Road
Cambridge CB3 OHE
ENGLAND

No. of
Copies

D. Lindley
Taylor Woodrow Construction, Ltd.
Taywood House
345 Ruislip Road
Southall
Middlesex UBI 2QX
ENGLAND

Dr. Neil Cherry
Lincoln College
Canterbury
NEW ZEALAND

ONSITE

DOE Richland Operations Office

D. R. Segna

39 Pacific Northwest Laboratory

J. C. Barnard (5)
J. W. Buck
J. R. Connell
D. W. Dragnich
C. E. Elderkin
D. L. Elliott
J. M. Hales
P. C. Hays
M. E. Hinchee
B. D. Holst
A. H. Miller
V. R. Morris
E. L. Owczarski
D. C. Powell
J. A. Stottlemyre
T. K. Thompson
R. E. Wildung
H. L. Wegley (5)
L. L. Wendell
Technical Information Files (5)
Publishing Coordination (2)
WCPE Program Dffice (5)